Proceedings of ASME Turbo Expo 2011
GT2011
June 6-10, 2011, Vancouver, Canada

GT2011-46012

AN INVESTIGATION OF TREATING ADIABATIC WALL TEMPERATURE AS THE DRIVING TEMPERATURE IN FILM COOLING STUDIES

Lei Zhao and Ting Wang
Energy Conversion and Conservation Center
University of New Orleans
New Orleans, LA 70148-2220, USA
Emails: lzhao@uno.edu; twang@uno.edu

ABSTRACT

In film cooling heat transfer analysis, one of the core concepts is to deem film cooled adiabatic wall temperature (T_{aw}) as the driving potential for the actual heat flux over the film-cooled surface. Theoretically, the concept of treating T_{aw} as the driving temperature potential is drawn from compressible flow theory when viscous dissipation becomes the heat source near the wall and creates higher wall temperature than in the flowing gas. But in conditions where viscous dissipation is negligible, which is common in experiments under laboratory conditions, the heat source is not from near the wall but from the main hot gas stream; therefore, the concept of treating the adiabatic wall temperature as the driving potential is subjected to examination. To help investigate the role that T_{aw} plays, a series of computational simulations are conducted under typical film cooling conditions over a conjugate wall with internal flow cooling.

The result and analysis support the validity of this concept to be used in the film cooling by showing that T_{aw} is indeed the driving temperature potential on the hypothetical zero wall thickness condition, ie. T_{aw} is always higher than T_w with underneath (or internal) cooling and the adiabatic film heat transfer coefficient (h_{af}) is always positive.

However, in the conjugate wall cases, T_{aw} is not always higher than wall temperature (T_w), and therefore, T_{aw} does not always play the role as the driving potential. Reversed heat transfer through the airfoil wall from downstream to upstream is possible, and this reversed heat flow will make $T_w > T_{aw}$ in the near injection hole region. Yet evidence supports that T_{aw} can be used to correctly predict the heat flux direction and always result in a positive adiabatic heat transfer coefficient (h_{af}).

The results further suggest that two different test walls are recommended for conducting film cooling experiments: a low thermal conductivity material should be used for obtaining accurate T_{aw} and a relative high thermal conductivity material be used for conjugate cooling experiment. Insulating a high-conductivity wall will result in T_{aw} distribution that will not provide correct heat flux or h_{af} values near the injection hole.

NOMENCLATURE

b	coolant injection slot width (mm)
h_{af}	adiabatic film heat transfer coefficient
l	chord length (mm)
M	blowing ratio, $(\rho u)_j/(\rho u)_g$
Nu_x	Nusselt number, hx/λ, x is the distance from the injection hole in streamwise direction
q"	heat flux (W/m^2), positive value for heat flowing from gas into the wall
Re_l	Reynolds number based on channel length, ul/ν
T_{aw}	adiabatic wall temperature (K)
T_w	wall surface temperature in contact with gas (K)
T_g	main gas flow temperature (K)
T_j	coolant temperature at the cooling jet hole exit (K)
T_{ci}	internal coolant temperature (K)
T_r	recovery temperature (K)

Greek Letters

η	adiabatic film cooling effectiveness, $(T_g-T_{aw})/(T_g-T_j)$
φ	film cooling effectiveness, $\varphi = (T_g-T_w) / (T_g-T_j)$ (or non-dimensional metal temperature, overall cooling effectiveness)

Subscripts

aw	adiabatic wall
ci	internal cooling
conj	conjugate blade
f	with film cooling
g	main flow of hot gas/air
j	coolant or jet flow
o	no film cooling
w	wall

INTRODUCTION

The efficiency of turbine engines improves as the turbine inlet temperature increases. Film cooling is one of the essential techniques utilized to reduce the airfoil temperatures and thermal stresses which tend to increase and are exacerbated as the turbine inlet temperature is continuously raised to augment gas turbine performance. Air bled from the compressor flows into the airfoils for internal cooling and then is ejected through small holes to form a layer of cooling film that blankets and protects the airfoil's surface from the hot mainstream gases. The film cooling jets consume valuable compressed air and therefore it is essential to continuously searching for new schemes to enhance film cooling performance and minimize the cooling mass flow through the jets.

Evaluation of film cooling performance in heat transfer is often based upon how much heat flux or blade temperature actually can be reduced after film cooling is employed. However, due to the experimental difficulty in directly measuring the heat flux, the **Heat Flux Ratio (HFR)** q'' / q''_o is often evaluated indirectly through a theoretical relation developed by Mick and Mayle [1] between two characteristic factors of film cooling heat transfer: adiabatic film effectiveness (η) and film heat transfer coefficients (h_{af} and h_o), as:

$$q'' / q''_o = (h_{af} / h_o)\,(1-\eta/\varphi) \qquad (1)$$

In which, the **adiabatic film effectiveness** is defined as:

$$\eta = (T_g - T_{aw}) / (T_g - T_j) \qquad (2)$$

η is an excellent indicator of film cooling performance by comparing the insulated wall surface temperature (T_{aw}) with the would-be perfect wall temperature, T_j. If the film cooling were perfect, $\eta = 1$ and the wall is protected as cold as the cooling jet temperature. The **adiabatic film heat transfer coefficient** is defined as:

$$h_{af} = q'' / (T_{aw} - T_w) \qquad (3)$$

where T_w is the airfoil wall surface temperature that comes immediately in contact with the hot main gas flow. In Eq. 1, the local heat flux without film cooling is given as:

$$q''_o = h_o\,(T_g - T_w) \qquad (4)$$

The **film cooling effectiveness**, φ, is defined as:

$$\varphi = (T_g - T_w) / (T_g - T_j) \qquad (5)$$

It needs to be noted that φ has also been called the **non-dimensional metal temperature** (The Gas Turbine Handbook [2]) or the **overall cooling effectiveness** in other literatures. The sign convention in this study is that a positive q" means heat flux moves into the wall from the gas stream.

For a perfect film cooling performance, the film cooling effectiveness would have a value of unity (η or $\varphi = 1.0$), i.e. the wall temperature (T_{aw} or T_w) is equal to the coolant temperature (T_j) at the exit of the jet injection hole; while a value of η ~~or φ~~ = 0 means that the film cooling has no effect in reducing the wall temperature, which is as hot as the mainstream gas. Note that under the condition in which film cooling is completely ineffective, φ is not necessarily equal to zero due to the effect of internal cooling or other cooling schemes.

In the film cooling heat transfer analysis mentioned above, one of the core concepts is to deem the film cooled adiabatic wall temperature (T_{aw}) as the driving potential for the actual heat flux over the film-cooled surface as proposed by R. J. Goldstein [3] in 1971. This concept can be approached in two ways. Firstly, T_{aw} can be simply treated as the highest temperature that the wall can possibly obtain when the wall is perfectly insulated. Hence, after the insulation is removed and the wall is subject to cooling underneath, the heat flux moves from the wall to the underneath cooling flow. This can be treated as being driven by the difference between T_{aw} and T_w. Secondly, theoretically the concept of treating the adiabatic wall temperature as the driving temperature potential is drawn from compressible flow when viscous dissipation becomes important and acts as a heat source to drive the heat flux. But, in conditions where viscous dissipation is negligible, which is common in experiments under laboratory conditions, the heat source is not from near the wall but from the main hot gas stream. It must be noted that the viscous dissipation phenomenon is fundamentally different from the physics in the film cooling condition. In follows that viscous dissipation is crucial, since dissipation is the actual energy source which converts the flow's kinetic energy to thermal energy near the wall; whereas in the film-cooling flow the only energy source is the hot gas stream (assuming viscous dissipation is negligible in the film-cooling flow discussed in this paper.) Therefore, the highest temperature value T_{aw} in the viscously dissipative flow is related to how much the converted thermal energy can be recovered by the wall via the recovery factor; whereas, in the film-cooling flow, the highest temperature that T_{aw} can possibly reach is T_g. Thus, using the concept of recovery factor (r) or recovering temperature (T_r) in the film-cooling flow to explain T_{aw} by some researchers seems artificial and shy of a support of flow physics if viscous dissipation is negligible. Lack of awareness of this difference has caused some confusion in explaining the film-cooling results. Therefore one of the objectives of this study is to examine whether the concept of treating adiabatic wall temperature as the driving potential in film cooling heat transfer is appropriate or not.

Harrison and Bogard [4] studied the validity of using T_{aw} as the driving temperature via the approach of comparing the heat flux and wall temperature of a film cooled wall using computed values of T_{aw} and h_f/h_o with the result from a conjugate model. They used the relative thickness between the velocity boundary layer and the thermal boundary layer to explain that if the thermal boundary layer is thinner than the velocity boundary layer, use of T_{aw} is acceptable; whereas if both boundary layers are of the similar thickness, then T_g instead of T_{aw} is the more appropriate driving temperature. Their observation and conclusion from the CFD results are not unexpected. Basically, their conclusion implies that T_{aw} is not always the driving temperature.

Considering that the passage of the heat flux in film cooling scenarios is from the only source (T_g) to the sink (coolant), it is reasonable to think that T_{aw} in the film-cooling flow doesn't represent the energy source (a cause) that drives the heat flow, but a "consequence" resulting from the thermal-flow fields. Since T_{aw} is just a result from the thermal-flow

field, the other options can also be considered to determine the driving temperature by examining the near wall local temperature field. For example, an effective temperature located between the wall and the core of coolant can be designated as the driving temperature as T_{eff} (x) = (T_g + f(x)T_j)/2, where f(x) is a function that describes the coolant core temperature attenuation along the streamwise direction. Apparently, f(x) is unknown and needs to be determined by experiments. However, a search for f(x) will further complicate the issue. This thought provokes the temptation to make it simple by just using the T_g as the driving temperature for all the film-cooling cases without trying to figure out what the effective local driving temperature would be along the wall.

A sketch is shown in Fig. 1 to qualitatively illustrate the heat transfer scenarios including the temperature profiles at two locations: one near the jet injection hole with a possible reversed heat flow in the airfoil base metal and the other located further downstream from the injection hole region. The slopes of the temperature profiles are drawn to qualitatively reflect the heat flow directions.

Examining Fig. 1 raises another question: theoretically, the T_{aw} used in Eq. 3 should be obtained with a perfect insulation of the surface. Will the conduction in the metal wall (or conjugate wall) affect the true value of T_{aw}? If it does, what is the deviation from the true T_{aw} value? This question has not been answered or even raised in previous film cooling studies involved with conjugate walls, such as papers published by Bohn et al. [5, 6, 7], Han et al. [8], Rigbi et al. [9] and Heidmann et al [10]. In summary, the conjugate wall effect on adiabatic wall temperatures has neither been noticed nor investigated in the previous studies.

The objective of this paper is to systematically investigate the above issues guided by CFD simulations.

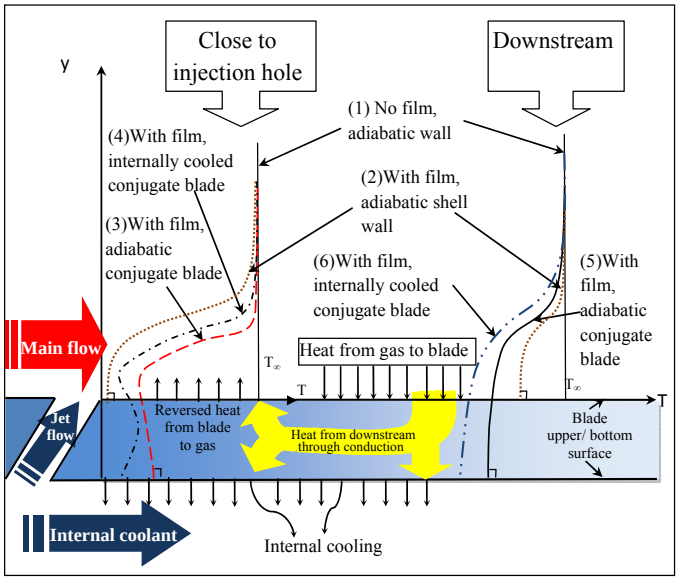

Figure 1 Qualitatively temperature profiles of a typical internally and film cooled blade at two locations: one near the injection hole region with potentially reversed heat transfer and the other located further downstream. The axial heat conduction transfer is small and the size of reversed heat flux arrowhead is enlarged for illustration purpose.

MODELING AND METHODOLOGY

The investigation in this paper is guided by a series of computational fluid dynamic (CFD) simulations. Although the actual numerical values of CFD are often subject to uncertainty due to different turbulence models, discretization resolution, and grid quality, the global heat transfer and flow physics can be captured relatively trustfully in modern CFD schemes. Since the focus of this study is on the thermal-flow physics and relative comparisons of different cases, any bias generated by the CFD scheme is generally not so critical in the comparative nature of the analysis conducted in this paper.

Considering experimental film cooling studies using low temperature and low heat flux laboratory conditions having been more commonly seen in open literatures than those employing real engine conditions, in this study, the issues will be discussed based on simulations of lab conditions first, followed by simulations in a representative engine operating condition.

Geometrical Configuration

To make analysis easier, 2D conditions with various changing parameters are simulated first. In 2D cases, a slot is selected; its configuration and the main dimensions are shown in Fig. 2. 3D simulation is then developed based upon the geometry set-up in the 2D studies, with a pitch to diameter ratio (p/b) of 3.

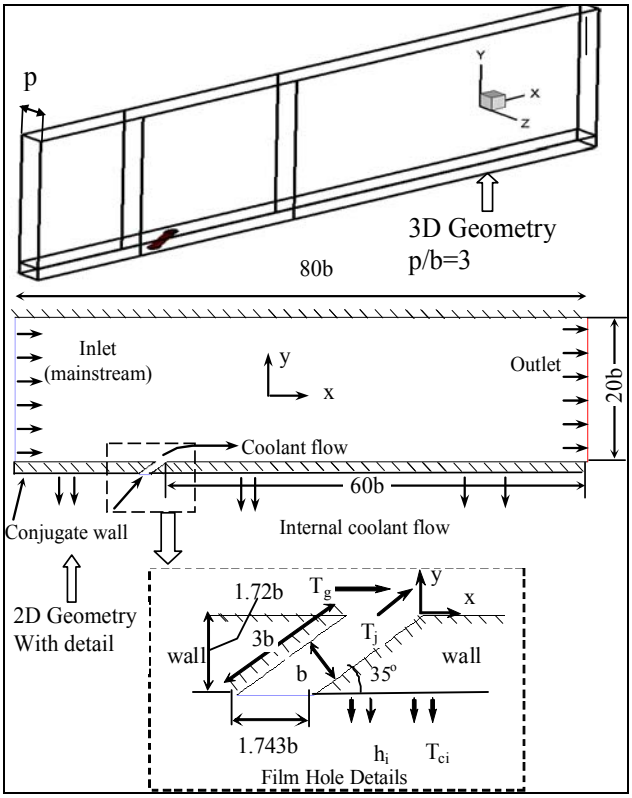

Figure 2 Computational domains for 2D and 3D respectively

The slot width (b) is 4 mm. The injection angle is 35°, which is considered as the optimal value by Bell et al. [11] and Brittingham et al. [12]. The length of the film slot is 3b from the coolant supply plenum to the surface. The computational domain has a length of 80b and a height of 20b. The slot jet is

set to 20b from the entrance of the mainstream. In the conjugate cases arrangement, the solid metal wall with a uniform thickness of 1.72b is included in the computational domain. An internal cooling channel flow is imposed below the base wall bottom surface, with an internal heat transfer coefficient h_i and a coolant flow temperature T_{ci} as shown in Fig. 2. It is understood that coolant plenum and film injection hole wall cooling conditions have important effects on film cooling performance. To simplify the analysis and focus on the T_{aw} issues, plenum is not included and adiabatic wall is assumed surrounding the wall of the film injection hole.

Governing Equations

The time-averaged, steady-state Navier-Stokes equations as well as equations for mass, energy and species transport are solved. The governing equations for conservation of mass, momentum, and energy are given as:

$$\frac{\partial}{\partial x_i}(\rho u_i) = S_m \tag{5}$$

$$\frac{\partial}{\partial x_i}\left(\rho u_i u_j\right) = \rho \bar{g}_j - \frac{\partial P}{\partial x_j} + \frac{\partial}{\partial x_i}\left(\tau_{ij} - \rho\overline{u'_i u'_j}\right) + F_j \tag{6}$$

$$\frac{\partial}{\partial x_i}\left(\rho c_p u_i T\right) = \frac{\partial}{\partial x_i}\left(\lambda \frac{\partial T}{\partial x_i} - \rho c_p \overline{u'_i T'}\right) + \mu\Phi + S_h \tag{7}$$

where τ_{ij} is the symmetric stress tensor defined as:

$$\tau_{ij} = \mu\left(\frac{\partial u_j}{\partial x_i} + \frac{\partial u_i}{\partial x_j} - \frac{2}{3}\delta_{ij}\frac{\partial u_k}{\partial x_k}\right). \tag{8}$$

$\mu\Phi$ is the viscous dissipation and λ is the heat conductivity.

Boundary Conditions

All walls have a non-slip velocity boundary condition in this study. Flow conditions with low temperature, pressure, and velocity for typical laboratory experiments are employed. For conjugate cases, Inconel X-750 properties were used for blade material with variable properties as functions of temperature. A heat transfer coefficient of h_i = 100 W/m^2-K and coolant flow temperature T_{ci} = 300K are assigned to the internal cooling flow, which is located at the bottom of Fig. 2. Variable fluid properties effect has also been included in the simulation. Air is modeled as an incompressible ideal gas with the density varying with temperature and the heat capacity modeled as a piecewise polynomial function of temperature with two temperature sub-ranges of 100-1000K and 1000-2000K, respectively. Inlet and outlet conditions, wall thermal boundary conditions for cases under lab conditions are summarized in Table 1.

Numerical Method

The commercial software code Fluent (version 6.2.16) from Ansys, Inc. is adopted in this study. The simulation uses the segregated solver, which employs an implicit pressure-correction scheme [13]. The SIMPLE algorithm is used to couple the pressure and velocity. Second order upwind scheme is selected for spatial discretization of the convective terms.

As shown in Fig. 3a, structured but non-uniform grids are constructed for 2D studies. The grids near the jet wall and the wall surface are denser than the other areas. A grid independence study was conducted by comparing adiabatic film effectiveness of simulations based on two different meshes of 80,000 and 48,000 cells respectively. The results are almost identical. The grid adopted in this study is of 400 cells in the x-direction and 120 in the y-direction for 2D studies. Unstructured grids are employed for the 3D studies with finer grids near the injection hole and the top surface. Less than 5% difference in adiabatic film effectiveness on centerline is found from the simulations based on meshes of 1.24 million cells versus 772,000 cells. Due to the limited RAM capability of the existing personal computers, the grid of 1.24 million cells is adopted in this study.

Converged results are obtained after the specified residuals are met. A converged result renders a mass residual of 10^{-5}, energy residual of 10^{-7}, and momentum and turbulence kinetic energy residuals of 10^{-6}. These residuals are the summation of the imbalance for each cell, scaled by a representative of the flow rate. Typically, 1000 to 2000 iterations are needed to obtain a converged result, which takes about 2 hours on a parallel computer cluster consisting of eight nodes of 2.53 GHz Pentium dual-core personal computers.

Table. 1. Summary of Boundary Conditions

Operational pressure	P (atm)	1	
Main stream inlet	T_g (K)	400	400K=260.6°F
	u_g(m/s)	10	Uniform
	Tu (%)	3	Turbulence Intensity
	Re_l x10^{-6}	0.21	l=0.32m
Jet inlet	T_j(K)	300	300 K = 80.6°F
	u_j (m/s)	10	Uniform
	Tu (%)	3	Turbulence intensity
	Re_d x10^{-3}	2.67	d=4mm
$M=(\rho u)_j/(\rho u)_g$	M	1.3	blowing rato
Outlet	P (atm)	1	Constant pressure
Conjugate cooling wall	T_{ci} (K)	300	
	h_i (W/m^2-K)	100	

CFD Model Qualification and Uncertainty Estimate

The effect of turbulence models using the same 2D mesh has been investigated in a previous study by Li and Wang [14]. The CFD results are in good agreement with the experimental result of Goldstein et al. [15] as shown in Fig. 3b. Enhanced near-wall treatment is employed and the Y^+ values from qualification case are below 0.8 for most X locations.

The uncertainty from the key factors are estimated as: 10% for the different turbulence models, 5% for turbulence length scales, 3% for resolution of second order central and upwind methods, 1% for convergence resolution, 5% for the effect of grid size, and 3% for the near-wall grid effect. The overall uncertainty for cooling effectiveness is estimated to be 13% with the root-mean-square method. The above uncertainty is estimated from the computational results under low temperature and pressure conditions. Therefore, the estimated uncertainty is not centered with the true value; rather it represents the uncertainty excursion of the results that are attributed by the computational model and scheme.

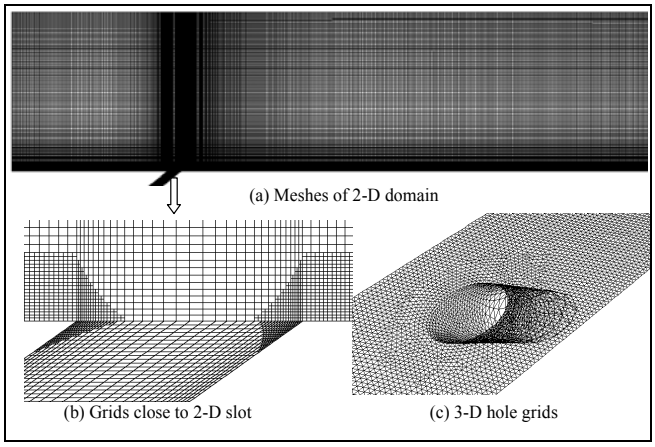

(a)

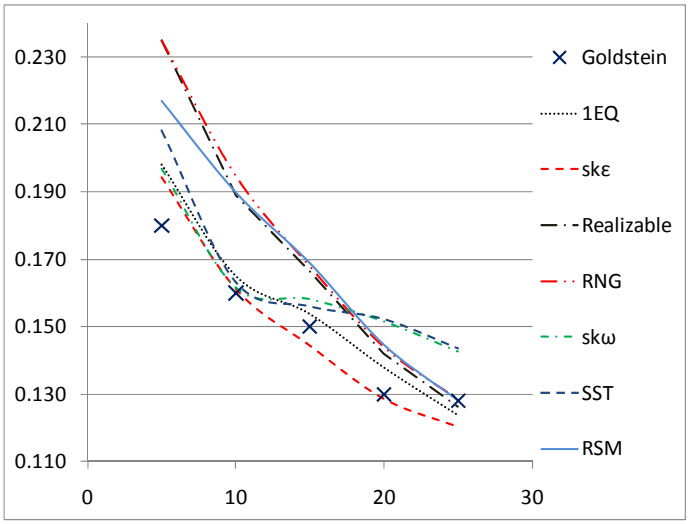

(b)

Figure 3 (a) Computational Meshes for 2D and 3D respectively (b) Comparison of CFD result with the experiment result of Goldstein [15]

Methodology and Cases Set-up

The conjugate heat transfer scenario of an operational turbine airfoil film cooling system consists of a main flow of hot gas with known conditions riding along the airfoil's upper surface, an internal coolant flow moving underneath the airfoil's bottom surface, and a portion of the coolant being injected through the coolant holes over the airfoil surface. The airfoil wall temperature and heat flux are determined by those conditions. The most appropriate simulation of this film-cooling system is to set up the main flow, internal flow and film injection conditions as boundary conditions while leaving the airfoil's wall thickness as part of the conjugate calculation.

To verify whether a temperature is the driving temperature, one vital feature is that the temperature should adequately predict the heat flux direction, i.e. heat should be driven into the airfoil surface when the driving temperature is higher than wall temperature and vice versa. Moreover, it can also be concluded that when wall temperature equals driving temperature, heat flux should be zero. From this point of view, two different approaches are taken in this study to investigate whether T_{aw} is the appropriate driving potential.

Approach One -- Comparing the sign of T_{aw}-T_w and the heat flux direction from simulation. In this approach, two groups of simulations are conducted separately: (1) film cooled adiabatic wall cases and (2) a film cooled conjugate wall case with internal cooling. The purpose of the adiabatic simulation (1) is to acquire T_{aw}, while the conjugate simulation (2) is to obtain T_w and the wall heat flux (q"). The evaluation of whether T_{aw} is the driving temperature is thus examined by checking whether $T_{aw} > T_w$.

Approach Two -- Comparing T_{aw} with the T_w where the heat flux is zero. In this approach, a constant temperature wall condition is imposed on the boundary. The location of the point where the wall heat flux is zero on the airfoil surface can then be identified, if it exists at all. From the discussion above, zero heat flux location only exists where the wall temperature equals the driving temperature. The T_{aw} at this specific location from the adiabatic simulation is then compared with the T_w. T_{aw} as the driving potential can be supported if good agreement with T_w is found. An illustration of Approach Two is shown in Fig. 4.

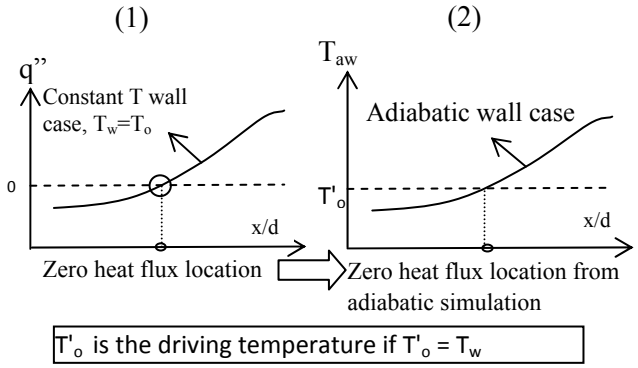

Figure 4 Illustration of Approach Two

A constant temperature wall condition is relatively difficult to maintain in real experiments, let alone the fact that many different temperature levels are involved in this study. But, it can be accomplished rather easily with the aid of CFD tools. The advantage of utilizing a CFD tool for this study is fully exploited and appreciated in executing Approach Two.

When considering the adiabatic airfoil condition, two options can be taken to simulate the adiabatic boundary condition: (1) **Shell wall** option --- the adiabatic wall condition is directly imposed on the wall surface in contact with the gas and the airfoil's wall thickness is not considered. (2) **Conjugate wall** option --- the adiabatic wall condition is applied to the inner (or bottom) surface of the airfoil and the airfoil's wall is included in the calculation. Option 1 is the ideal case for achieving the perfect adiabatic condition. The T_{aw} obtained from Option 1 is what is supposed to be used in Eqs. 2 and 3. Option 2, in turn, is the actual condition in experiments as well as in the real turbine airfoils due to the necessity of installing a finite-thickness wall and the convenience of directly applying insulation on the test section's outer surface. It would be interesting to use CFD to find out the difference of T_{aw} obtained from these two different approaches, and indentify the effects of the conjugate wall on T_{aw}.

The simulated cases of this study are summarized in Table 3 and illustrated in Fig. 5. Case 1 (adiabatic shell wall case) is set as the baseline case.

Table 3 Summary of Cases Set-up

Case #	Thermal Boundary Condition	Dimen
Case 1	Adiabatic wall, shell wall (Baseline Case)	2D
Case 2	Adiabatic wall, conjugate wall	2D
Case 3a	Internal cooling, conjugate wall	2D
Case 3b	Internal cooling, shell wall	2D
Case 4.1	Constant Tw=305K, shell wall	2D
Case 4.2	Constant Tw=315K, shell wall	2D
Case 4.3	Constant Tw=325K, shell wall	2D
Case 5	Adiabatic wall, shell wall	3D
Case 6.1	ConstantTw=320K, shell wall	3D
Case 6.2	Constant Tw=350K, shell wall	3D
Case 6.3	Constant Tw=380K, shell wall	3D
Case 7a	Internal cooling, conjugate wall	3D
Case 7b	Internal cooling, shell wall	3D

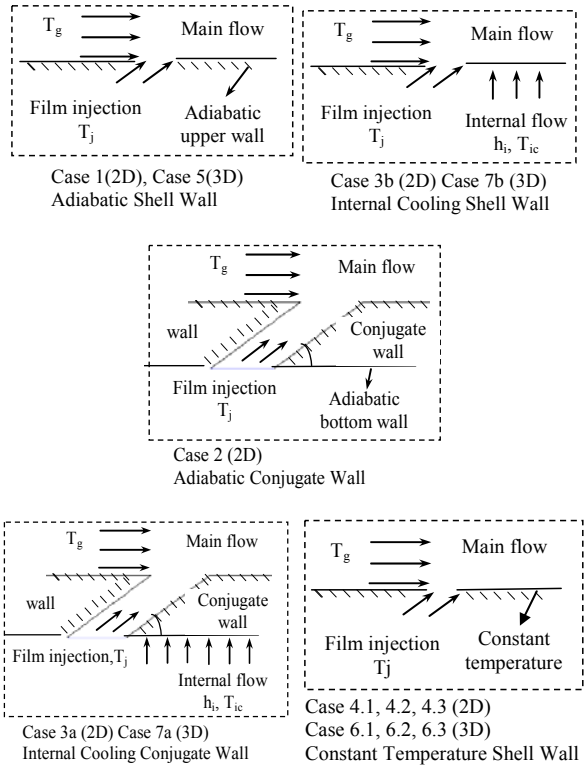

Figure 5 Illustrations of boundary condition and wall thickness treatment for different cases

RESULTS AND DISSCUSSIONS

Effect of Conjugate Wall on Adiabatic wall temperature

Before discussing the concept of T_{aw} as the driving temperature potential, how T_{aw} should be obtained needs an attention. In developing the film heat transfer theory, the adiabatic wall condition is directly imposed on the wall surface in contact with gases without including the wall thickness (i.e. the **shell wall concept**). But in typical experimental procedures of obtaining the adiabatic wall temperature, insulation is installed outside the test surface. Thus, the airfoil's wall thickness has always been included naturally in T_{aw} measurement. To examine the effect of conjugate wall, simulations of Cases 1, 2, 3a and 3b in 2–D were carried out. The results of η, and φ are plotted in Fig.6. All the wall temperatures and heat fluxes shown in Fig. 6 are referred to the surface contacting the hot gas (or the top surface of the conjugate wall).

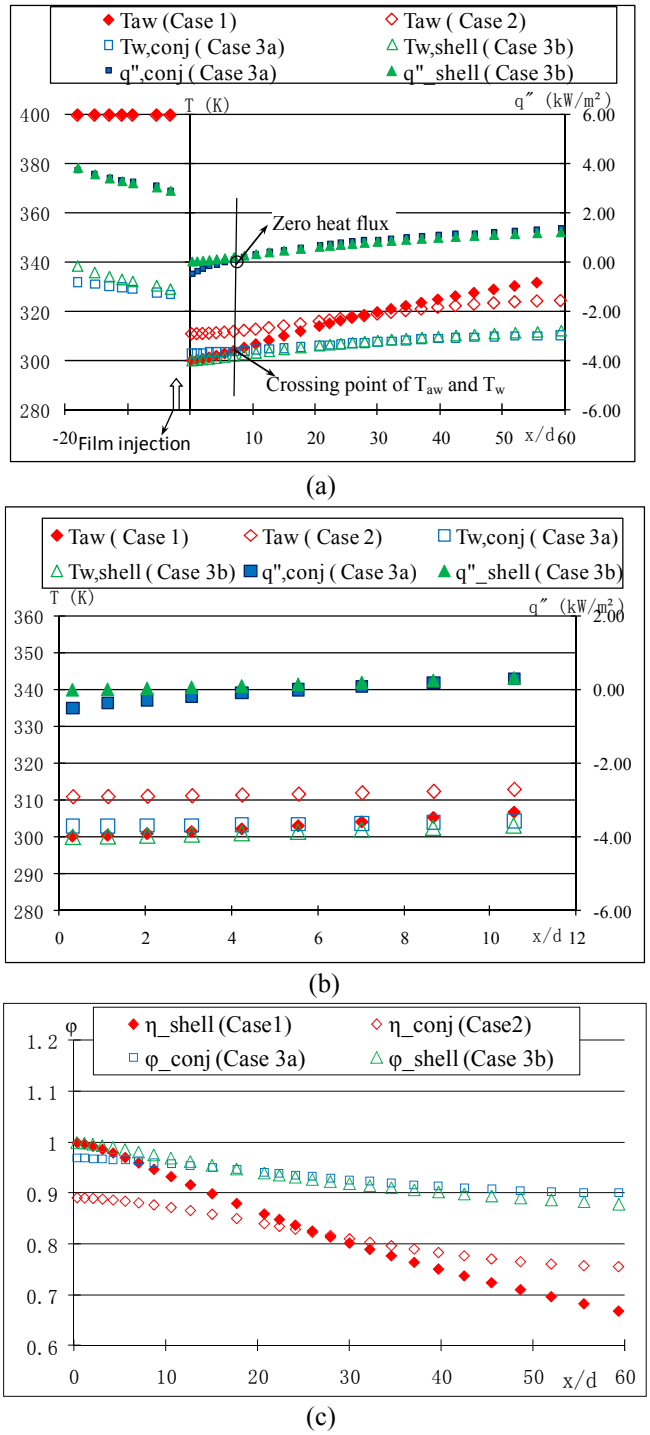

Figure 6 (a) Adiabatic wall temperatures, conjugate wall temperature and heat flux in two y-axes (b) Zoom-in view of (a) in near injection hole region (c) Film cooling effectiveness (φ) and adiabatic film cooling effectiveness (η)

From Fig.6 (a), it is noticed that the adiabatic wall temperature with conjugate wall (Case 2) is more uniformly distributed across the airfoil surface than adiabatic shell wall

case (Case 1). T_w curves of Cases 1 and 2 cross over at around x/d=30. Due to the finite wall thickness and the good conductivity of metal, heat transfer inside the wall from the hotter, downstream region to the upstream, cooler region is not negligible, so the overall wall temperature distribution of Case 2 (adiabatic conjugate wall) is "smeared" to become more uniform than Case 1 (adiabatic shell wall), with higher temperatures in the near-hole region and lower temperatures in the downstream area. The bottom wall temperature of Case 2 (not shown here) is only about 1°C cooler than the top surface due to the thin thickness of the wall. For this specific case, the wall thickness of 1.72d yields about a 12 percentage point increase of maximum η near the film hole and about a 5 percentage point reduction of η farther downstream (x/d > 50).

To further investigate the wall heat conduction effect, a low thermal conductivity wood is used to replace the metal wall. The CFD result shows T_w of the wood wall is almost identical to Case 1's shell wall approach. Since the data of these two cases coincide with each other, the wood wall is not shown here. This proves the importance of including a metal wall with appropriate thermal conductivity as the airfoil material in both the experimental and computational analysis of the film cooling study to obtain adequate results.

To verify whether a temperature is the driving temperature, two criteria must be satisfied simultaneously: (a) the driving temperature should be higher than the wall temperature, i.e. $T_{driving} - T_w > 0$, (b) ($T_{driving}$- Tw) and the heat flux should have the same sign, i.e. h_{af} is always positive in Eq. 3. The goal here is to examine if T_{aw} is $T_{driving}$.

In Fig.6 (a), first examine Case 3 (internally cooled conjugate wall) temperature distribution, and then compare it with the adiabatic Cases 1 and 2. Again the "smearing" effect of the wall through conduction in Case 2 is noticed, and as a result T_{aw} from Case 2 is first higher then lower than T_{aw} from Case 1. It is noted that in most parts of the airfoil, T_{aw} (Cases 1 and 2) is higher than T_w of Case 3, so if T_{aw} is the driving temperature, the heat should flow from the gas into the wall. Examination of the heat flux curve in Fig. 6 does show the heat flux of Case 3 is positive. It is further noticed that the heat flux flips to the negative direction (i.e. moving from the wall to the gas) at x< 6D near the crossing point of T_w of Cases 1 and 3. In this case, the heat flux direction is consistent with the sign of T_{aw}-T_w : when $T_{aw}>T_w$, positive heat flux is found (heat moves from the gas to the wall) and when $T_{aw}<T_w$, the heat flux is negative, moving from the wall to gas. This reversed heat transfer direction ($T_w > T_{aw}$) indicates that **T_{aw} is not always the driving temperature in conjugate wall** cases, although T_{aw} still serves an important role as the adequate "reference" temperature to determine the heat flux direction. This characteristics of T_{aw} will result in an always positive value of h_{af} in Eq. 3.

If the wall conduction is the culprit that has caused T_w to be greater than T_{aw}, what would happen if the wall is included in the adiabatic wall simulation? This is done in Case 2 by applying the adiabatic condition on the bottom wall. Figure 6 (a) and (b) shows that T_{aw} in Case 2 is always higher than T_w in Case 3a (internal cooling, conjugate wall) and Case 3b (internal cooling, shell wall) throughout the entire region downstream of the film, i.e. criteria (a) of the driving temperature is satisfied. In this condition, it is predicted that no heat flux direction change should occur if T_{aw} from Case 2 is the driving temperature, but as discussed earlier, the heat flux in Case 3a changes sign at x/d=5.6 in Fig.6, indicating that negative h_{af} values exist and criteria (b) is not satisfied. This also implies that using T_{aw} obtained from insulating **the bottom wall of a conjugate case** (Case 2) does not always work out well as the driving temperature and neither does T_{aw} always serve well as a reference temperature to accurately indicate the heat flux direction. Recall that the T_{aw} obtained from the shell wall (Case 1) is not always higher than T_w, but it serves well as the adequate reference temperature to indicate the correct heat flux direction and results in an always positive h_{af} in Eq. 3.

Usually, T_w should be always lower than T_{aw} if the wall thickness were negligibly thin. Since the wall thickness and the accompanied heat conduction are not negligible in the conjugate case, heat flows from downstream hotter region to the near-hole colder region and heats the wall temperature to a level higher than T_{aw}. Therefore, theoretically, it seems the concept of treating T_{aw} as the driving temperature still holds if the wall thickness is zero with cooling.

To examine this hypothesis, Case 3b is conducted with internal cooling on a shell wall. Fig. 6 clearly shows that all the T_{aw}'s obtained on the shell wall in Case 1 are higher than the T_w's obtained from shell wall in Case 3b and all the heat fluxes are positive. **Thus it is concluded that T_{aw} is indeed the driving potential in film cooling cases with zero wall thickness.**

In summary, the shell wall T_{aw} is not always higher than T_w in the conjugate wall case, the concept of treating T_{aw} as the driving temperature is not supported under the conjugate wall condition. However, T_{aw} is an important reference temperature that provides the correct information for determining the heat flux direction and always produces a positive h_{af} value. "Reference temperature" means it serves as the "reference" that is compared with T_w to determine the heat flux direction. For example, $T_{aw} > T_w$ results in heat flux moving from the gas to the wall and vice versa. On the other hand, the T_{aw} of the adiabatic conjugate wall case is always higher than T_w of the internally cooled conjugate wall case, but the heat flux direction is not always consistent with treating T_{aw} as the driving temperature and the h_{af} value can become negative in the region where reverse heat flux is present. Therefore, in the real experimental condition for obtaining T_{aw}, it is recommended that the test wall be built with a material having a very low thermal conductivity plus insulation. The T_{aw} obtained in this condition will be closer to the theoretical value of T_{aw} as would be obtained from the shell wall condition. However, when T_w or h_o, or ϕ of Eqs. 3,4 and 5 are to be obtained from the experiment, it is recommended that a material with similar thermal conductivity as the airfoil's metal be used. This means two different test walls are recommended for film cooling experiments: a low thermal conductivity material be used for obtaining accurate T_{aw} and a relative high thermal conductivity material be used for the conjugate cooling experiment. Insulating a high-conductivity wall will result in a T_{aw} distribution similar to Case 2, which will not provide correct heat flux or h_{af} values near the injection hole.

An Alternate Method to Examine T_{aw}'s Role under a Constant T_w Condition

Due to the complexity of the conjugate wall condition, an alternate examination is conducted by imposing the constant

wall temperature condition on the 2D shell wall as in Cases 4.1, 4.2, and 4.3. Through the numerical simulations, the location where zero wall heat flux occurs on the airfoil surface can be identified. From the previous discussion, it can be derived that a zero heat flux point exists when the wall temperature equals the driving potential. Thus, the advantage of using the constant wall temperature condition lies on the fact that it makes the selection of the actual driving temperature at the zero heat flux location easier than the previous conjugate wall case where the wall temperature varies. Meanwhile T_{aw} at the same location can be obtained from the previously conducted adiabatic shell wall study. By comparing this with the actual driving temperature, the physical role that T_{aw} plays in film cooling heat transfer can be appropriately evaluated.

The heat flux and wall temperatures from Cases 4.1, 4.2, and 4.3 together with the T_{aw} from the baseline case are shown in Fig. 7 with the heat flux plotted on the secondary y-axis on the right. Again it is found that the heat flux direction can be predicted fairly well using T_{aw} as the reference temperature. The actual driving temperatures are plotted with the corresponding T_{aw} in Fig. 8 and the values are documented in Table 4. It is shown that T_{aw} is very close to the actual driving temperature in all three cases. The difference is less than 3% scaled by T_g-T_j. The results prove again that T_{aw} plays the role as a good reference temperature that can be used to identify the correct heat flux direction with an always positive h_{af} value when it is compared with the surface temperature, even under the artificial boundary condition of various constant wall temperatures. This means that if the wall temperature is artificially assigned higher than T_{aw}, heat must be provided to the wall, which heats the gas stream.

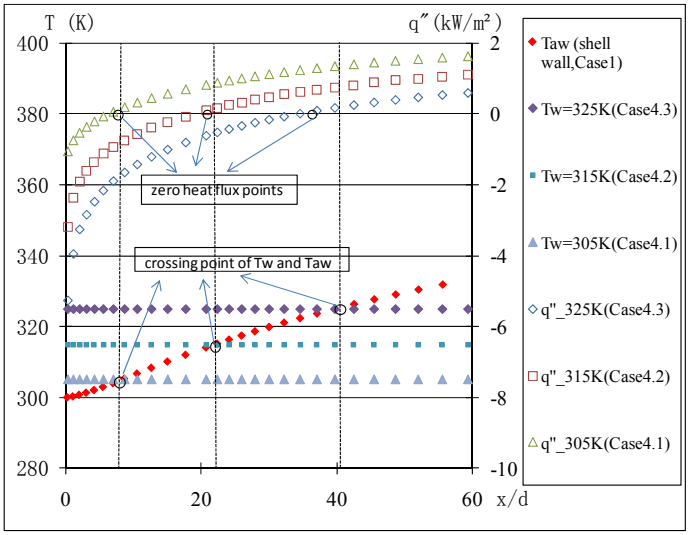

Figure 7 Heat flux, wall temperatures from Cases 4.1, 4.2 and 4.3 with T_{aw} from the baseline case (Case1)

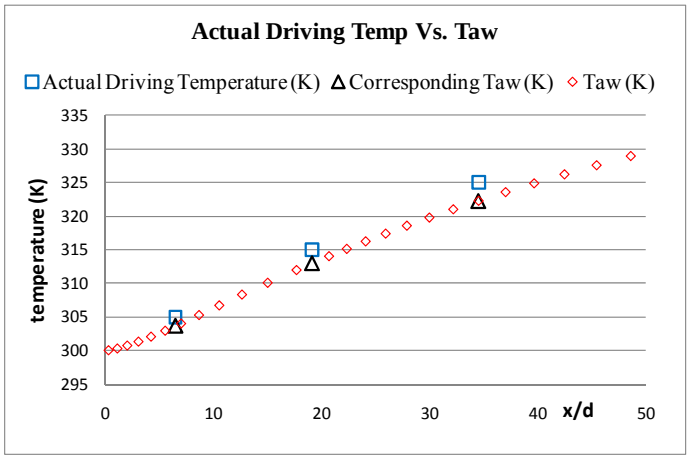

Figure 8 Comparison between the actual driving temperature and T_{aw} in the 2D Study

Table 4 The actual driving temperature and corresponding T_{aw} in 2D studies

Zero heat flux location	Actual driving Temperatu	Corresponding Taw (K)	(T_actual-Taw)/(T∞-Tj)
6.51	305	303.67	1.33%
19.17	315	313.01	1.99%
34.58	325	322.29	2.71%

3D Studies

In the previous 2D studies, it is shown that T_{aw} represents the actual driving temperature very closely and also heat flux direction can be accurately predicted by using T_{aw} as the reference temperature. The role of T_{aw} is re-examined when more complex flow mixing is introduced by 3D simulations. The adiabatic shell wall condition case is studied in Case 5 followed by the constant temperature wall cases 6.1, 6.2 and 6.3 with different wall temperatures. Similar to 2D studies of Case 4a and 4b, conjugate wall (Case 7a) and shell wall (Case 7b) cases in 3D with internal cooling are then simulated to investigate T_{aw} as the driving temperature. The heat fluxes and wall temperatures at the mid-planes from Cases 6.1, 6.2, and 6.3 and Cases 7a and 7b, together with the T_{aw} from Case 5 along the centerline through the center of the hole are shown in Fig. 9 (a) and (b) with the heat flux plotted on the secondary y-axis on the right. For the convenience of comparison, T_{aw} from the 2D studies is also drawn in the same figure.

Comparing T_{aw} in 3D cases with 2D cases, it is found that the 3D cases produce a much higher T_{aw} than the 2D cases. Also, it is noticed that T_{aw} in a 3D case is more uniform for most of the surface than in the corresponding 2D case, with the exception of the region near the injection hole where a steep temperature gradient is found. The difference is due to the distinct different characteristics of flow fields in 2D versus 3D cases, as can be seen in Fig. 10. In 2D cases, film does not have a quick "escape" mechanism, so that the coolant flow typically spreads over the blade surface generating a relatively ideal protecting film. Heat from the hot main flow must penetrate into the film layer first and then passes onto the blade surface. On the other hand, in 3D cases the mixing between the film layer and the main flow is fueled with lateral coherent-structure

mixing through kidney vortices (with axes coming out of the paper), making the film heat up more quickly and is thus less effective in protecting the surface than in 2D cases. The kidney vortices' flow structure is demonstrated in Fig. 11 at different locations for Case 5 (3D adiabatic shell wall). Moreover, since the coolant film only covers part of the blade around the centerline (Fig. 12), hot main flow penetrates in between film coverage (from multiple film injection holes) and is further entrained and wrapped toward the surface from the lateral direction. All those factors, stronger mixing and lateral wrapping (or "side-leaking"), contribute to a more uniform temperature but less effective film cooling in 3D cases than 2D cases.

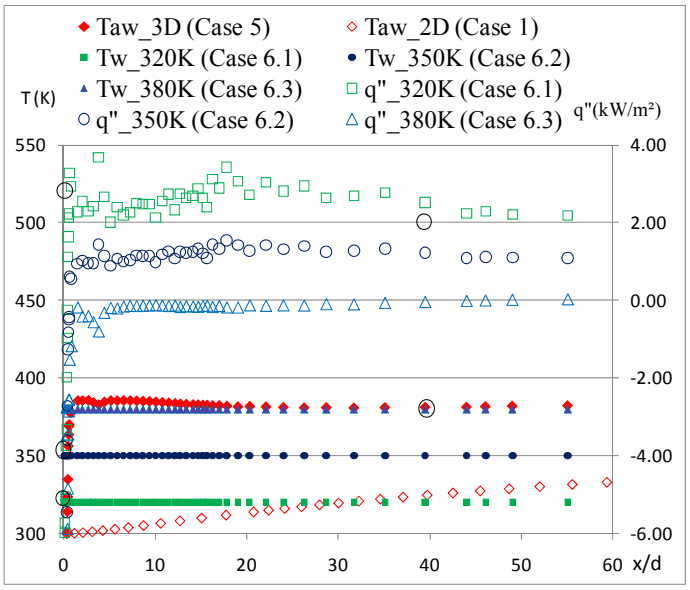

(a)

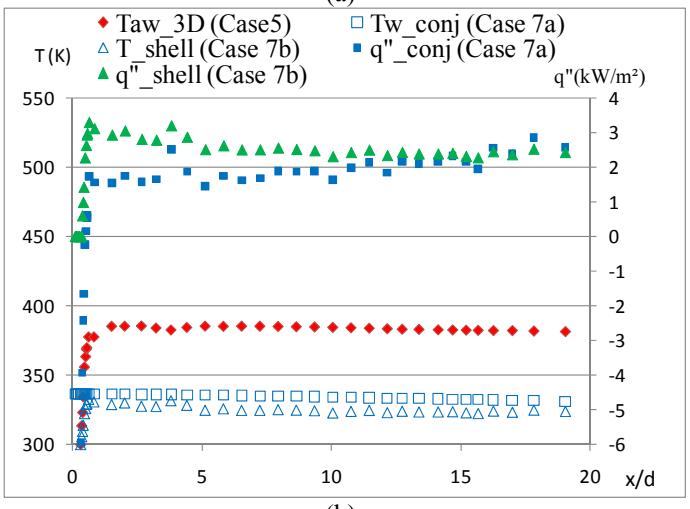

(b)

Figure 9 Heat flux, wall temperatures from 3D Cases (a) Cases 6.1, 6.2 and 6.3 (b) Cases 7a and 7b. T_{aw} along the centerline through the center of the hole from the 3D baseline case (Case5) and 2D baseline case (Case1) also included for comparison. Heat flux plotted on secondary axis on the right.

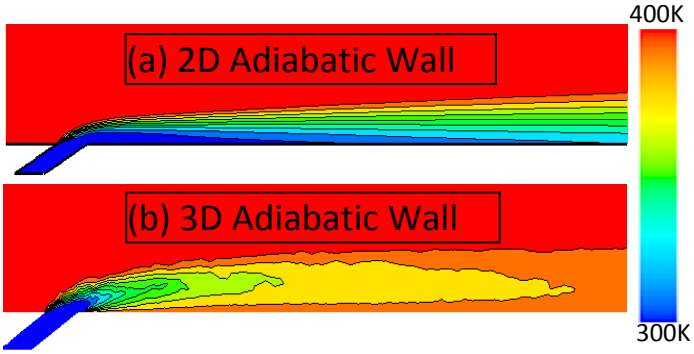

Figure 10 Test surface temperature contours of Case 3 (2D) and Case 5 (3D)

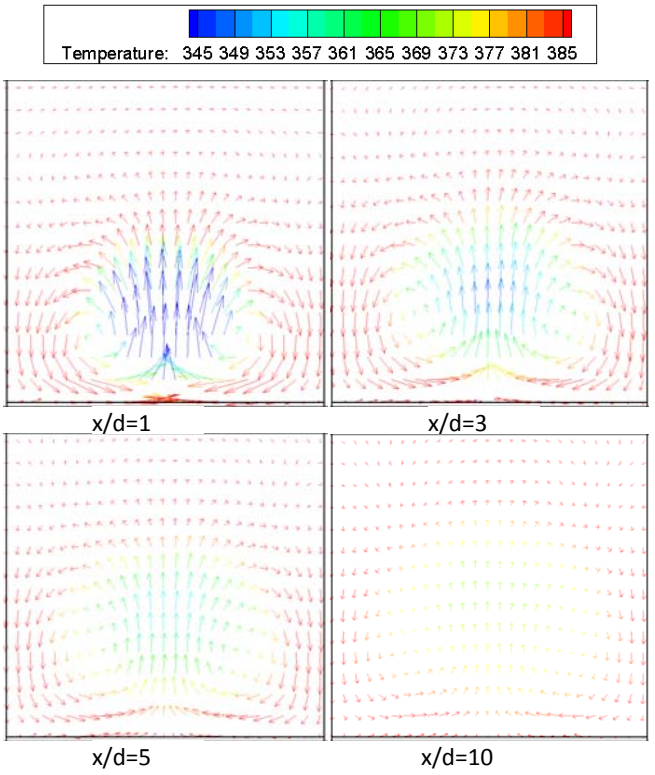

Figure 11 Velocity vector plot for Case 5 at different locations

Similar to 2D studies, a reversed heat flux region is also seen with heat transferring from the hotter section to cooler sections in the conjugate wall and further heating the cooler gas near the surface. But, this reverse heat flux region is smaller than in 2D cases due to the stronger mixing effect in 3D simulations. Even though the T_{aw} pattern is quite different between 2D and 3D cases, again it is found that the heat flux direction can be predicted fairly well using T_{aw} as the reference temperature. This implies that the h_{af} value will be always positive even when the heat flux changes direction. The actual driving temperatures are also plotted with the corresponding T_{aw} in Fig. 13 and the values are shown in Table 5. T_{aw} is shown very close to the actual driving temperature in Case 6.3 (less than 2% deviation) but is off by about 15% and 20% in Cases 6.1 and 6.2, respectively.

It is concluded that even though the flow structure is more complex under 3D conditions, the roles of T_{aw} are identical as

in the 2D cases, ie. T_{aw} is the driving temperature under the ideal shell wall condition; however, with the heat conduction in the metal wall, T_{aw} doesn't always drive the heat flux, but it performs well as the reference temperature to determine the heat flux direction and produces an always positive h_{af} value.

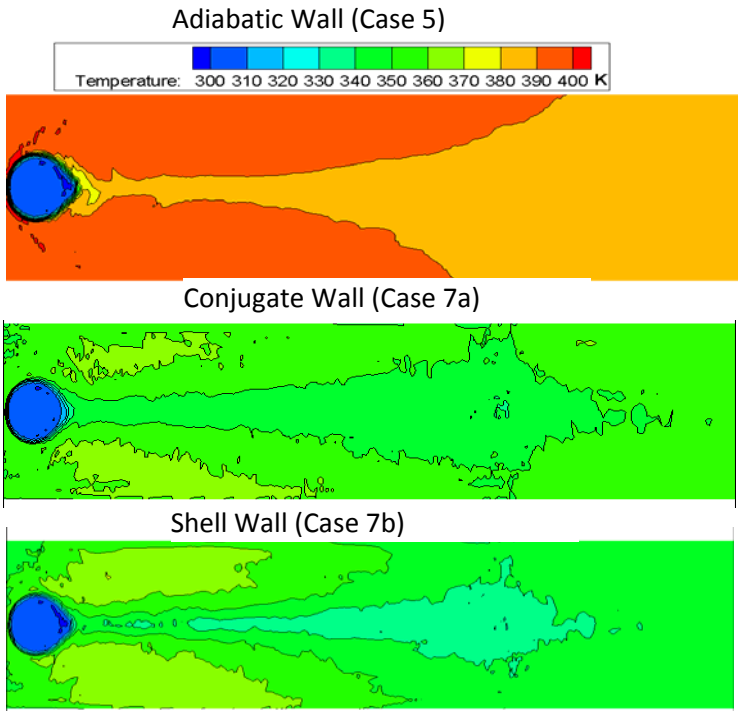

Figure 12 Test surface temperature contours of Case 5, Case 7a and 7b

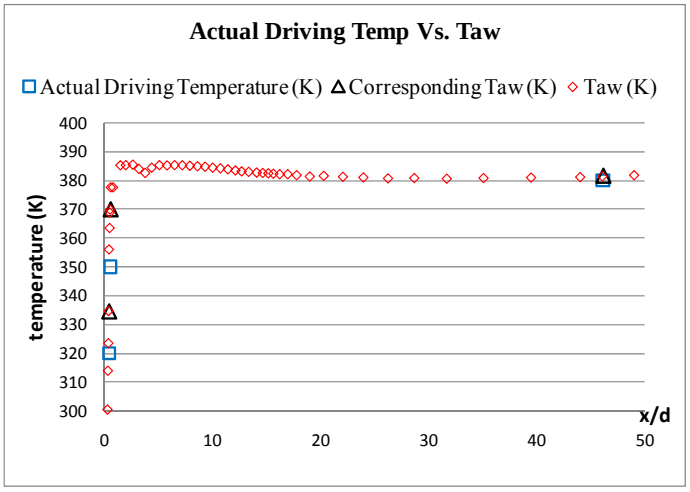

Figure 13 Comparison between the actual driving temperature and T_{aw} in 3D Study

Table 5 T_{aw} comparing with actual driving temperature in 3D studies

Zero heat flux location (x/d)	Actual driving Temperature (K)	Corresponding Taw (K)	(T_actual-Taw)/(T∞-Tj)
0.42	320	334.7	-14.70%
0.56	350	370	-20.00%
46.1	380	381.6	-1.60%

CONCLUSION

In this study, the appropriateness of employing the concept of treating the adiabatic wall temperature, T_{aw}, as the driving temperature was first questioned because the heat source is from the main hot gas stream, not coming from the near-wall viscous dissipation like in the compressible flow condition. However, the analysis supports the validity of this concept to be used in film cooling by showing that **T_{aw} is indeed the driving temperature potential on the shell wall (zero wall thickness) condition,** ie. T_{aw} is always higher than T_w with underneath (or internal) cooling and h_{af} is always positive. However, when the conjugate wall condition is imposed as in the actual airfoil film cooling application, a reverse heat condition occurs in the metal wall by transferring heat from the downstream hotter section to the cooler region near the injection hole, resulting in a hotter wall condition ($T_w > T_{aw}$) with heat transfer from the wall to the gas. This means that T_{aw} cannot be treated as the driving temperature anymore; nonetheless, T_{aw} stills plays another important role as the reference temperature that can be utilized to correctly determine the heat flux direction and always result in positive h_{af} values including the condition involving reversed heat flux flowing from the wall to the gas due to conduction in the wall. These conclusions are valid in both 2D and 3D flow conditions although the 3D flow is more complex in nature.

The above conclusions also imply that the physics of conjugate wall conduction and cooling is important and needs to be simulated in both experiment and CFD analysis to obtain the correct heat transfer coefficient, heat flux, and film cooling effectiveness. Wall conduction smears the temperature distribution and reduces film cooling effectiveness. However, in order to use the measured T_{aw} correctly, the test wall should be made of very low-conductivity material, reinforced with a good insulation to approach the shell wall (zero wall thickness) condition. The film cooling test condition built with a finite-thickness conjugate wall with thermal conductivity similar to the metal base of an airfoil is appropriate to measure the heat transfer coefficient and film cooling effectiveness, but less appropriate for conducting adiabatic film cooling experiments because the heat conduction in the finite wall will "mess up" the true physics of true T_{aw} and result in a negative h_{af} value in the region where reverse heat flux is present.

ACKNOWLEDGEMENT

This study is supported by the Louisiana Governor's Energy Initiative via the Clean Power and Energy Research Consortium (CPERC) and administered by the Louisiana Board of Regents.

REFERENCE

[1] W.J. Mick, R.E. Mayle, Stagnation film cooling and heat transfer, including its effect within the hole pattern, ASME J. of Turbomachinery 110 (1988) 66-72.

[2] The Gas Turbine Handbook, Office of Fossil Energy, National Energy Technology Laboratory, U.S. Department of Energy, 2006, PP. 310-318.

[3] R.J. Goldstein, Film cooling advances in heat transfer 7 (1971) 321-379.

[4] K. Harrison, and D.G. Bogard, Use of the adiabatic wall temperature in film cooling to predict wall heat flux and temperature, ISROMAC Paper 12 (2008) 20187.

[5] D. Bohn, B. Bonhoff, H. Schonenborn, H. Wilhelmi, Prediction of the Film-cooling Effectiveness of Gas Turbine Blades Using a Numerical Model for the Coupled Simulation of Fluid Flow and Diabatic Walls, AIAA paper 95-7105, 1995

[6] D. Bohn, B. Bonhoff, H. Schonenborn, "Combined Aerodynamic and Thermal Analysis of a Turbine Nozzle Guide Vane," IGTC-paper-108, Proc. of the 1995 Yokohama Int. Gas Turbine Congress, 1995

[7] D. Bohn, V. Becker, K. Kusterer, Y. Otsuki, T. Sugimoto, R. Tanaka, "3-D Internal and Conjugate Calculations of a Convective Cooled Turbine Blade with Serpentine-shaped and Ribbed Channels," IGTI paper 99-GT-220, 1999.

[8] Z. Han, B. Dennis, G. Dulikravich, "Simultaneous Prediction of External Flow-Field and Temperature in Internally Cooled 3-D Turbine Blade Material," IGTI paper 2000-GT-253, 2000.

[9] J. Heidmann, D. Rigby and A. Ameri, A Three-Dimensional Coupled Internal/External Simulation of a Film Cooled Turbine Vane, ASME paper 99-GT-186, 1999.

[10] D. Rigby and J. Lepicovsky, Conjugate Heat Transfer Analysis of Internally Cooled Configurations, ASME paper 2001-GT-0405, 2001.

[11] C.M. Bell, H. Hamakawa1, P.M. Ligrani, Film cooling from shaped holes, ASME J. Heat Transfer, 122 (2000) 224-232.

[12] R.A. Brittingham, J.H. Leylek, A detailed analysis of film cooling physics: Part IV—compound-angle injection with shaped holes, ASME J. Turbomachinery 122 (2002) 133-145.

[13] Fluent Manual, Version 6.2.16, Fluent, Inc. 2005.

[14] X. Li and T. Wang, Effects of various modeling on mist film cooling, ASME Journal of Heat Transfer 129 (2007) 472-482.

[15] R. J. Goldstein, P. Jin, and R. L. Olson, Film Cooling Effectiveness and Mass/Heat Transfer Coefficient Downstream of One Row of Discrete Holes, J. Turbo mach. 121 (1999), 225-232